In situ observed relationships between snow and ice surface skin temperatures and 2 m air temperatures in the Arctic

Pia Nielsen-Englyst[1], Jacob L. Høyer[1], Kristine S. Madsen[1], Rasmus Tonboe[1], Gorm Dybkjær[1], Emy Alerskans[1]

[1]Danish Meteorological Institute, DK-2100 Copenhagen Ø, Denmark

Correspondence to: Pia Nielsen-Englyst (pne@dmi.dk)

Abstract.

To facilitate the construction of a satellite derived 2 m air temperature (T2m) product for the snow and ice covered regions in the Arctic, observations from weather stations are used to quantify the relationship between the T2m and skin temperature (Tskin). Multiyear data records of simultaneous Tskin and T2m from 29 different in situ sites have been analysed for 5 regions, covering the lower and upper ablation zone and the accumulation zone of the Greenland Ice Sheet (GrIS), sea ice in the Arctic Ocean, and seasonal snow covered land in northern Alaska. The diurnal and seasonal temperature variabilities and the impacts from clouds and wind on the T2m-Tskin differences are quantified. Considering all regions, T2m is on average 0.65-2.65°C higher than Tskin, with the largest differences for the lower ablation area and smallest differences for the sea ice sites. A negative surface radiation balance generally makes the surface colder than the atmosphere, resulting in a surface-driven surface air temperature inversion. Tskin and T2m are often highly correlated, and the two temperatures are almost identical (<0.5°C) at particularly times of the day and year, and during certain conditions. The data analysed here show the best agreement between Tskin and T2m around noon and early afternoon during spring and fall. However, Tskin is often lower than T2m by more than 2°C, with the largest differences occurring, when it is cold or when the surface is melting. In general, the inversion strength increases with decreasing wind speeds, except for the sites on the GrIS where the maximum inversion occurs at wind speeds of about 5 m s^{-1} due to the katabatic winds. Clouds tend to reduce the vertical temperature gradient, by warming the surface, resulting in a mean T2m-Tskin difference ranging from -0.08°C to 1.63°C, with the largest differences for the low ablation zone sites and the smallest differences for the seasonal snow covered sites. To assess the effect of using cloud limited Infrared satellite observations, the influence of clouds on temporally averaged Tskin has been assessed by comparing averaged clear-sky Tskin with averaged all-sky Tskin. The clear-sky effect has been assessed for temporal averaging windows of: 24 h, 72 h and 1 month. The largest clear-sky biases are generally found when 1 month averages are used and smallest for 24 h. In most cases all-sky averages are warmer than clear-sky averages, with the smallest bias during summer.

1 Introduction

The Arctic region is warming about twice as much as the global average because of Arctic amplification (Graversen et al., 2008). Greenland meteorological data show that the last decade (2000s) is the warmest since meteorological measurements of surface air temperatures started in the 1780s (Cappelen, 2016; Masson-Delmotte et al., 2012) and the period 1996-2014 yields an above average warming trend compared to the past six decades (Abermann et al., 2017). The reason for the Arctic amplification is a number of positive feedback mechanisms, e.g. the ice-albedo feedback which is driven by the retreat of Arctic sea ice, glaciers, and terrestrial snow cover. The atmospheric warming leads to a declining mass balance of the Greenland Ice Sheet (GrIS), contributing to global sea level rise. The increased mass loss of the GrIS partly comes from increased surface melt (Rignot, 2006), which is driven by changes in the surface energy balance. Several studies have focussed on the assessment of current albedo trends and their possible further enhancement of the impact of atmospheric warming on the GrIS (e.g. Box et al., 2012; Stroeve et al., 2013; Tedesco et al., 2011). However, recent studies have shown that uncorrected sensor degradation in MODIS Collection 5 data was contributing falsely to the albedo decline in the dry snow areas, while the decline in wet and ice areas remain but at lower magnitude than initially thought (Casey et al., 2017). Future projections of the GrIS mass balance show that the surface melt is exponentially increasing as a function of the surface air temperature (Franco et al., 2013). Further, the Arctic warming may contribute to mid latitude weather events (Cohen et al., 2014; Overland et al., 2015; Vihma, 2014; Walsh, 2014). It is therefore important to monitor the temperature of the Arctic to understand and predict the local as well as global effects of climate change. Current global surface temperature products are fundamental for the assessment of the climate change (Stocker et al., 2014) but in the Arctic these data traditionally include only near surface air temperatures from buoys and automatic weather stations (AWSs; Hansen et al., 2010; Jones et al., 2012; Rayner, 2003). However, in situ observations are not available everywhere and the time series have gaps and/or limited duration. In particular, the Arctic ice regions are sparsely covered with in situ measurements, due to the extreme weather conditions and low population density (Reeves Eyre and Zeng, 2017). The global surface temperature products are thus based on a limited number of observations in this very sensitive region. This means that crucial climatic signals and trends could be missed in the assessment of the Arctic climate changes due to poor coverage of the observational system.

Satellite observations in the thermal infrared have a large potential for improving upon the surface temperature products in the Arctic due to the good spatial and temporal coverage. However, the variable retrieved from infrared satellite observations is the surface skin temperature (Tskin), whereas current global surface temperature products estimate the 2 m air temperature (T2m; Hansen et al., 2010; Jones et al., 2012). An important step towards integrating the satellite observations in the near surface air products is thus to assess the relationships between Tskin and T2m as we do here.

A surface-based air temperature inversion is a common feature of the Arctic winter (Serreze et al., 1992; Zhang et al., 2011). The inversion exists because of an imbalance between the radiative fluxes, leading to a cooling of the surface, especially when the absorbed incoming solar radiation is small (during winter and night). An analysis based on observations from the

Antarctic Plateau showed that the inversion continues all the way to the surface with the largest gradient between the surface and 20 cm above it (Hudson and Brandt, 2005). The surface-driven temperature inversion causes a difference between the T2m and the actual skin temperature at the snow/air interface. Previously, work has been done to characterize the relationship between the T2m and land surface temperatures observed from satellites and identified land cover, vegetation fraction and elevation as the dominating factors (Good et al., 2017). A few studies have investigated the temperature inversion in the ice regions for the lowest 2 m of the atmosphere focusing on limited time periods and single locations e.g. Summit, Greenland (Adolph et al., 2018; Hall et al., 2008), the South Pole (Hudson and Brandt, 2005) and the Arctic sea ice (Vihma and Pirazzini, 2005). Until now, no systematic studies have yet been made for the high latitude ice sheets and over sea ice.

The difference between the T2m and Tskin is very important in validation studies of remotely sensed temperatures. Several studies have used T2m observations for validating satellite Tskin products on the GrIS (Dybkjær et al., 2012; Hall et al., 2008; Koenig and Hall, 2010; Shuman et al., 2014) and over the Arctic sea ice (Dybkjær et al., 2012) and found that a significant part of the differences could be attributed to the difference between the Tskin and T2m. Conversely, Rasmussen et al. (2018) used satellite Tskin observations in a simple way to correct the T2m in a coupled ocean and sea ice model and obtained an improved snow cover.

In order to facilitate the integrated use of Tskin and T2m from in situ observations, satellite observations and models, there is a need for a better understanding and characterization of the observed relationship. The aim of this paper is to bring further insight into this relationship, using in situ observations. This study extends the previous analyses to include multiyear observational records from 29 different sites located at the GrIS, Arctic sea ice, and the coastal region of northern Alaska. The aim is to identify the key parameters influencing the temperature difference between the surface and 2 m height and to assess under which conditions Tskin is, or is not, a good proxy for the T2m and to quantify the differences, using Tskin as a proxy for T2m. The findings are intended to aid the users of satellite data and to support the derivation of T2m using satellite Tskin observations. In the response to the latter, an effort has also been made to estimate a clear-sky bias of Tskin based on in situ observations. The paper is structured such that Sect. 2 describes the in situ data. Section 3 gives an introduction to the near surface boundary conditions. The results are presented in Sect. 4 and discussed in Sect. 5. Conclusions are given in Sect. 6.

2 Data

In situ observations have been collected from various sources and campaigns covering ice and snow surfaces in the Arctic. The focus has been on collecting in situ data with simultaneous observations of Tskin, derived from infrared radiometers and T2m measured with a shielded and ventilated thermometer about 2 m above the surface. Table 1 gives an overview of the data and the abbreviations used in this paper. The data has been divided into five different categories based on surface characteristics and location: accumulation area (ACC), upper/middle ablation zone (UAB), lower ablation zone (LAB) of the

GrIS, seasonal snow covered (SSC) sites in northern Alaska, and sea ice sites (SICE). All time series which cover multiple full years have been cut to cover an integer number of years (within 5 days), in order to avoid seasonal biases. The geographical distribution and elevations of all sites are shown in Fig. 1, while Fig. 2 shows the temporal data coverage. Observations from the sites in Table 1 include T2m, Tskin, wind speed, shortwave- and longwave radiation. Measurement heights vary depending on the site and snow depth, but for this paper near-surface air temperatures are referred to as 2 m air temperature despite these variations. The impact of these height variations are discussed in Sect. 5. Further details are provided for each data source in Sect. 2.1-2.6.

2.1 PROMICE

Data have been obtained from the Programme for Monitoring of the Greenland Ice Sheet (PROMICE) provided by the Geological Survey of Denmark and Greenland (GEUS). PROMICE was initiated in 2007 by the Danish Ministry of Climate and Energy, and operated by GEUS in collaboration with the National Space Institute at the Technical University of Denmark and Asiaq (Greenland Survey; e.g. Ahlstrøm et al., 2008). PROMICE collects in situ observations from a number of AWSs mostly located along the margin of the GrIS (Fig. 1). Each observational site has one or more stations; typically one located in the lower ablation zone close to the ice sheet margin, and one or two located in the middle/upper ablation zone near the equilibrium line altitude. Exceptions are KAN_U and KPC_U located in the lower accumulation area and EGP, which is located in the upper accumulation area. All 22 PROMICE AWSs located on the GrIS have been used in this study. PROMICE Tskin has been calculated from up-welling longwave radiation, measured by Kipp & Zonen CNR1 or CNR4 radiometer, assuming a surface longwave emissivity of 0.97 (van As, 2011). The air temperature is measured by a thermometer at a height of 2.7 m, while the wind speed is measured at about 3.1 m height, if no snow is present. Snow accumulation during winter reduces the measurement height. In this study, we use hourly averages of the data, provided by PROMICE.

2.2 ARM

The Atmospheric Radiation Measurement (ARM) Program (Ackerman and Stokes, 2003; Stamnes et al., 1999) was established in 1989 and it provides data on the cloud and radiative processes at high latitudes. Three ARM sites from the North Slope of Alaska (NSA) are used in this study: Atqasuk (ATQ), Barrows (BAR), and Oliktok Point (OLI). The stations provide surface snow infrared (IR) temperature measured using a Heitronics KT19.85 IR Radiation Pyrometer (Moris, 2006) and air temperature measured at 2 m height. Wind speed is measured at 10 m height. The ARM stations have seasonal snow coverage, i.e. the snow melts away in summer. Data where the surface albedo is less than 0.30 indicate that the snow has disappeared and these have been excluded to ensure that we only consider snow/ice covered surfaces.

2.3 ICEARC

We use the ICEARC sea ice temperature and radiation data set from the Danish Meteorological Institute (DMI) field campaign in Qaanaaq. The DMI AWS is deployed on first-year sea ice in Qaanaaq and is funded by the European climate research project, ICE-ARC. The AWS was deployed for the first time in late January 2015 at the north side of the fjord Inglefield Bredning and recovered in early June before break-up of the fjord ice. The campaign has been repeated every year since then and the data used in this study is procured by fieldwork done in the periods Jan.-Jun., 2015-2017. The AWS is equipped to measure snow surface IR temperature and air temperature at 1 and 2 m heights. In this study, the 1 m air temperature is used instead of the 2 m air temperature, as careful analysis of the 2 m air observations revealed anomalies that could arise from a systematic temperature dependent error. Using the 1 m instead of 2 m air temperatures observations will have an impact on the strength of the relationship with the Tskin observations, but the observations are included here as the dependency with other parameters, such as cloud cover and wind, is still important to assess. The data used here are 10 minute snapshots (Høyer et al., 2017) and are referenced as: DMI_Q in this paper.

2.4 SHEBA

The Surface Heat Budget of the Arctic (SHEBA) experiment was a multiagency program led by the National Science Foundation and the Office of Naval Research. The data used in this study originates from deployment of a Canadian icebreaker, DesGroseilliers, in the Arctic ice pack 570 km northeast of Prudhoe Bay, Alaska in 1997 (Uttal et al., 2002). During its year-long deployment, SHEBA provided atmospheric and sea ice measurements from the icebreaker and the surrounding frozen ice floe. The data used here contain hourly averaged data collected by the SHEBA Atmospheric Surface Flux Group (ASFG) and Dr. J. Liljegren from the ARM project. The SHEBA ASFG installed a 20 m tall tower, which was used to obtain measurements of the surface energy budget, focusing on the turbulent heat fluxes and the near surface boundary layer structure (Bretherton et al., 2000; Persson, 2002). Five different levels, varying in height from 2.2-18.2 m, had mounted a temperature/humidity probe and a sonic anemometer. We use air temperature and wind data from the lowest mounted instruments (2.2 m), which vary in height from 1.9 to 3 m depending on snow accumulation and snow melt. Three surface temperature measurements were measured from a General Eastern thermometer, an Eppley radiometer and a Barnes radiometer, available from April to September 2007. The Eppley is the most reliable, though there are periods when the other two are also reasonable, and one period (May), when the Eppley data may be slightly off (Persson, 2002). We use the best estimate of Tskin, which is based on slight corrections to the Eppley temperatures and the Barnes temperatures when Eppley was known to be wrong (Persson, 2002).

2.5 FRAM2014/15

The scientific program of the FRAM2014/15 expedition is carried out by the Nansen Center (NERSC) in co-operation with Alfred Wegener Institute, Helmholtz Centre for Polar and Marine Research, Germany, University of Bergen, Bjerknes

Center for Climate Research and Norwegian Meteorological Institute. FRAM2014/15 is a Norwegian ice drift station deployed near the North Pole in August 2014 using a medium-sized hovercraft as logistic and scientific platform (Kristoffersen and Hall, 2014). This type of mission allows exploration of the Arctic Ocean not accessible to icebreakers, and enables scientific field experiments, which require physical presence. The hovercraft was operated by two people and by the end of March 2015 they had drifted 1.450 km. During the drift with sea ice they obtained Tskin measurements by Campbell Scientific IR120 (later corrected for sky temperature and surface emissivity) and near surface air temperature from a temperature sensor.

2.6 TARA

TARA is a French polar schooner that was built to withstand the forces from the Arctic sea ice. In late August 2006 TARA sailed to the Arctic Ocean, where she drifted for fifteen months frozen into the sea ice. The TARA multidisciplinary experiment was a part of the international polar year DAMOCLES (Developing Arctic Modelling and Observing Capabilities for Long-term Environmental Studies) program (Gascard et al., 2008; Vihma et al., 2008). Air temperature and wind speed were measured from a 10 m tall Aanderaa weather mast at the heights of 1, 2, 5, and 10 m and wind direction was measured at 10 m height. We use the air temperatures and wind speed measured at 2 m height. They also had an Eppley broadband radiation mast with two sensors for longwave fluxes and two sensors for shortwave fluxes (upward and downward looking). The downward looking IR sensor also provided Tskin from April to September 2007. The data used in this study are 10 minute averages.

2.7 Radiometric observations of Tskin

The Tskin observations used in this study are all derived from radiometric observations, but with spectral characteristics that range from the Heitronics KT19.85 with a spectral response function from 9.5-11.5 μm over Campbell Scientific IR120 with a 8-14 μm spectral window to broadband longwave observations from ~4-40 μm. The emissivity of the ice surface varies for the different spectral windows and this leads to a difference in actual observed Tskin as the sky temperature, which is reflected, tends to be much colder than the ice surface in the infrared, in particular during cloud free conditions. The contribution from the reflected sky is thus included in the radiometric observations but the ice and snow surfaces have generally very high emissivities, which reduce the effects from the reflected sky radiation. In Høyer et al. (2017), the difference in emissivity between the KT15.85 and the IR120 was modelled using an IR snow emissivity model with the spectral response functions for the two types of instruments (e.g. Dozier and Warren, 1982). This resulted in averaged emissivities of 0.998 for the KT15.85 and 0.996 for the IR120 spectral windows for a typical snow surface and an incidence angle of 25 degrees. Using the same type of model for a broadband 4-40 μm spectrum resulted in an emissivity of 0.997. The high emissivities for all three instruments mean that the contributions from the sky are small. For realistic conditions in the

Arctic, this e.g. introduces an average difference of 0.06°C between the IR120 and the KT15.85 radiometer (which has a similar spectral response function as the KT19.85), with the IR120 being colder than the KT15.85 (Høyer et al., 2017).

Several of the stations (ATQ, BAR, OLI, DMI_Q, SHEBA and FRAM) used here observed both narrow band and wide band IR observations of the ice surface. The two types of Tskin have been calculated and compared for each of the stations. Figure 3 shows an example with a comparison of the two Tskin estimates from DMI_Q. There is close to a 1:1 relation between the two observations, meaning that there are no systematic temperature dependencies in the comparison. Considering all sites, a good agreement if found with a mean difference between the two Tskin types of 0.06°C and a mean root mean squared value of 0.96°C. In the following we use the narrow band Tskin observations when available and the broadband at the other stations and assume that all the Tskin derived observations have the same characteristics.

2.8 Longwave-equivalent cloud cover fraction

For each site, the cloud cover fraction (CCF) has been estimated based on the relationship between T2m and down-welling longwave radiation (LW_d), following the cloud cover estimation already included in the PROMICE data sets (van As, 2011; van As et al., 2005). It is based on Swinbank (1963), who presented a very simple approach for estimation of clear-sky (CCF=0) atmospheric longwave radiation as a function of T2m:

$$LW_{d\_clear} = 9.365 \cdot 10^{-6} \cdot \mathrm{T2m}^2 \cdot \sigma \cdot \mathrm{T2m}^4, \qquad (1)$$

where σ is Stefan-Boltzmann's constant. Overcast conditions (CCF=1) are assumed to occur when the observed LW_d exceeds the blackbody radiation emitted from the surface, which is calculated using T2m. The CCF for any observed T2m and LW_d pair from all individual observation sites is then calculated by linear interpolation of the observed LW_d, between the theoretical clear-sky (from Equation 1) and the overcast estimates. See van As (2011) for more details on the CCF calculation.

3. Introduction to the near surface boundary conditions

To perform an analysis of the Tskin and T2m relationship and interpret the results it is important to consider the surface energy balance and the specific characteristics that apply in the Arctic. The surface temperature and surface melt are driven by the surface energy balance. The net surface energy balance is defined by the fluxes of energy between the atmosphere, the snow/ice surface and the underlying land, snow/ice, or ocean. The surface energy balance can be written

$$SW_d - SW_u + LW_d - LW_u + SH + LH + G = M,$$

where M is the net energy flux at the surface and SW_d, SW_u, LW_d, LW_u, SH, LH, and G represent the down- and upwelling shortwave radiation, down- and upwelling longwave radiation, sensible and latent heat flux, and subsurface conductive heat flux, respectively. The energy fluxes have the unit W m^{-2}. All fluxes are positive when energy is added to the surface. A positive net surface energy balance results in warming of the surface, if the temperature is lower than the freezing point of water, or in melting of snow and ice (latent heat) if the temperature is at the freezing point. When the surface energy balance

is negative the snow/ice will cool thus driving the conductive heat flux from warmer layers below. If the surface is melting, a negative energy balance results in freezing of liquid water.

The radiative budget of the polar regions is dominated by longwave radiation during much of the year and even during summer the shortwave radiation input is in the same order of magnitude as the incoming longwave radiation flux because of extensive cloud cover especially during late summer, and the high surface albedo of the snow (Maykut, 1986). SW_d is the dominating source for ice melt in Greenland (van den Broeke et al., 2008; Box et al., 2012; van As et al., 2012), even though non-radiative energy fluxes can dominate during shorter periods (Fausto et al., 2016). On average, the non-radiative fluxes are an order of magnitude smaller than the radiation fluxes. However, because the net radiation balance is small compared to the individual radiation fluxes the variations in SH and LH fluxes are important for the total surface energy balance and thus the surface temperature. Surface winds interact strongly with the surface energy fluxes as the turbulent mixing increases as a function of wind speed (van As et al., 2005).

During winter and clear-skies when *SWd* is negligible, *LWu* is higher than the *LWd*. This drives a positive sensible heat flux and it results in a stable stratification of the lower atmospheric boundary layer (Maykut, 1986). When the heat conduction flux from below is limited on thick sea ice and on continental ice sheets the negative radiation budget at the surface makes the surface temperature colder than the surface air temperature, resulting in a surface-based temperature inversion. At low to moderate wind-speeds, when turbulent mixing is limited, this creates a very stable stratification of the lower atmosphere. On a sloping surface, the surface air starts to flow downslope, driven by the existence of a horizontal temperature gradient and gravity. The generated winds are called inversion or katabatic winds, and are characterised by stronger winds at more negative surface net radiation and a strong correlation between slope and wind direction (Lettau and Schwerdtfeger, 1967). In the case of PROMICE sites on GrIS, we will refer to these winds as katabatic winds and in the case of interior Antarctic studies these winds are referred to as inversion winds for consistency with referenced studies.

Clouds play a complex role in the Arctic surface energy budget e.g. they both reflect SW_d, leading to a cloud shortwave cooling effect, and absorb LW_u and emit LW_d, which tend to have a warming effect. In the Arctic clouds have a predominantly warming effect on the surface (Intrieri, 2002; Walsh and Chapman, 1998) as the dry atmosphere, with lower emissivity and with that absorptivity to *LW* radiation, enhances the cloud longwave warming effect, while the high surface albedo and the high solar zenith angles thus the impact of the cloud shortwave cooling effect (Curry et al., 1996; Curry and Herman, 1985; Zygmuntowska et al., 2012).

4 Results

4.1 Diurnal and seasonal temperature variability

The local air and surface temperature conditions in the Arctic are to a large extent influenced by the length of the day or night in the Arctic, with extreme variations depending on latitude and time of the year. The temperature variability has several important temporal scales. In this study we will focus on the diurnal and seasonal temperature variations, which are

key temporal scales of variability, considering the aim of deriving T2m from satellite observations. As an example of the large seasonal variations, Fig. 4 shows the 2014 monthly mean diurnal temperature variation of Tskin and T2m at the upper PROMICE site in Kangerlussuaq, KAN_U, during January, April, July and October. The seasonal variability in the diurnal temperature at KAN_U is representative of the conditions at the other stations, except for the general temperature level at each station, which changes with latitude and altitude. Considering all months individually, there is high correlation between Tskin and T2m ranging from an average value of 0.92 in January to an average of 0.99 in July considering the entire time series of KAN_U. The high correlations arise from hourly variability and daily cycles in temperatures that are seen in both temperature records. The correlation decreases for stations which have occasional surface melt, where Tskin is constrained to the freezing point of water. Both Tskin and T2m reach a maximum in July, while the coldest month is December (not shown). During winter and polar night, there is no clear diurnal cycle in either T2m or Tskin, and T2m is higher than Tskin. However, during spring there is a strong diurnal cycle, with Tskin lower than T2m at night and small T2m-Tskin differences during daytime. The shadings indicate the standard deviations in T2m and Tskin, respectively. The largest variability is found in spring and winter as a result of more frequent and rapid passages of cold and warm air masses in contrast to the summer months (Steffen, 1995). The summer temperature variability is moreover limited by the upper limit of 0°C on Tskin when the surface melting begins.

The large seasonal variations in Fig. 4 and the relationship between T2m and Tskin are typical for all sites. Figure 5a shows the monthly mean Tskin for all sites and all years. EGP is by far the coldest site due to its high elevation, with a monthly mean Tskin of -42°C in January and a maximum of -11°C in July. All sites reach a maximum in Tskin in July, regardless of latitude. July is also the month with least variation in temperature among sites, where melt at most stations (exception is ACC sites) constrains Tskin, while the winter months show a larger variance in Tskin among sites since local conditions are dominating Tskin. The AWS data from the GrIS show the effect of altitude and latitude on Tskin, with the high altitude sites being the coldest (EGP, KAN_U and KAN_M) together with the most northern sites (THU_U and KPC_U). The southern (e.g. QAS_A and QAS_U) and low altitude sites (most LAB sites, TAS_U, TAS_A) occur to be the warmest. The SICE sites are comparable in temperature with the coldest sites on the GrIS (except from EGP), but are slightly warmer in summer and fall.

Figure 5b shows the mean daily range (daily max – daily min difference) of Tskin as a function of month for all sites and all years. Again, the observations show a similar pattern across the diverse geographical locations. During summer, the high elevation sites tend to have the largest daily range in Tskin, while the observations from LAB and SICE sites show the smallest daily range. This is very likely an effect of the warmer temperatures and the Tskin upper temperature limit at 0°C, the melting point for ice. This constraint is seen during summer at almost all data records included in this study (exceptions are the ACC sites). Figure 5c shows the mean difference between T2m and Tskin for all observation sites as a function of time of year. In general, the SICE sites show the weakest inversion, while the LAB sites show the strongest inversion. For the ACC sites the weakest inversion is found during summer, while the LAB sites tend to have the strongest inversion during summer. This is explained by differences in surface conditions during summer, where the LAB sites have surface melt in

contrast to the high elevation ACC sites, where the surface warms but not reaches the ceiling of variability (the melting point).

Figure 5 indicates both yearly and daily variations in the observed Tskin and T2m relationship. A detailed analysis of these variations can be seen in Figures 6a-b, which illustrate the mean diurnal and seasonal T2m-Tskin differences for the ACC and LAB sites, respectively. The SSC and SICE sites have not been included as none of the individual sites have a continuous data record throughout the year without gaps. As also noticed in Fig. 4, the winter months have very little diurnal variability in the T2m-Tskin difference, with an approximately constant difference of about 1.5-2.5°C for the LAB sites and 0.5-1.5 °C for the ACC sites. During spring and summer the differences decrease at the ACC sites and the weakest vertical stratification is found around noon or early afternoon, where Tskin may even exceed T2m slightly resulting in an unstable stratification of the surface air column. For the LAB sites, the weakest stratification is found in spring and fall, around noon and early afternoon. The summer months show large differences due to the constrain of Tskin for melting surfaces, which is common to all LAB sites. At night the net radiation is negative, thus cooling the surface resulting in a surface-based inversion for both surface types. The T2m-Tskin differences are higher (especially in summer) at the LAB sites compared to the ACC sites, and the UAB sites have temperature differences in between. The reason for the higher temperature difference at the lower altitude sites is the longer time periods with surface melt.

4.2 Impact from wind

The surface wind speed is an important component in the near surface thermal stratification since the turbulent mixing increases as a function of wind speed (Monin and Obukhov, 1954). Figure 7 shows how the wind regimes differ among the observation sites used in this study. In general, winds on the GrIS are strongest in winter and reach a minimum around July (see also Steffen and Box, 2001). The surface radiative cooling and the terrain play the primary role in the generation of the surface winds. The direction and strength of the prevailing surface winds are closely related to the direction and steepness of the slope and the strength of the inversion. Surface winds at the PROMICE sites generally have a high directional persistence (see Fig. 4 in van As et al., 2014), commonly blowing from inland, which is an indication that local winds are often katabatic winds. High elevation sites experience stronger winds due to the larger radiative cooling of the surface (provided a comparable surface slope is present; Fig. 8; van As et al., 2014). The SSC and SICE sites show less variability in wind speed on annual basis. At these sites the wind is determined by large scale synoptic conditions combined with local topography.

The expectation is that stronger inversions can develop in low wind speed conditions because of reduced turbulent mixing. Figure 8a-b shows the T2m-Tskin difference as a function of binned wind speed. The middle plots show the binned distribution of the T2m-Tskin difference (with bin size of 1 K) as a function of binned wind speed, where the colour bar is the number of members in each bin. The top plots show the mean (solid lines) and standard deviation (dashed lines) of the T2m-Tskin difference as a function of the binned wind speeds. Figure 8a shows data from the DMI_Q AWS on sea ice. As expected, the strongest temperature inversion occurs at low wind speeds and larger wind speeds have larger turbulent mixing

and thus smaller vertical temperature differences between Tskin and T2m. However, THU_U (Fig. 8b) shows that this relationship is more complex. The maximum inversion is reached at wind speeds from 3-5 m s^{-1}, whereas the mean and standard deviation decrease for calm winds (<2.5 m s^{-1})

The wind dependencies shown in Fig. 8 are representative for all the stations in this paper, where the SICE and the SSC sites resemble Fig 8a and all the PROMICE stations have a wind dependency similar to Fig. 8b. The pattern is explained by the inversion combined with a surface slope that results in a flow, which actually destroys its own forcing and as a result there is an optimum in inversion strength and wind speed. The PROMICE behaviour is also found by Adolph et al. (2018) at the Summit station on the GrIS. Miller et al. (2013) also found that the surface based inversion intensity peaks at wind speeds ranging from 3 to 10 m s^{-1} at Summit based on microwave radiometer retrieved profiles. Furthermore, Hudson and Brandt (2005) show that at the South Pole the maximum inversion strength occurs at wind speeds of 3-5 m s^{-1}. They suggest that it is not the weak wind of 3-5 m s^{-1} that promotes the strong inversion, but the inversion which forces the air flow resulting in an inversion wind. They investigated this using the model by Mahrt and Schwerdtfeger (1970), which relates the slope of the terrain and the strength of the inversion to the inversion wind. Their results supported the idea that the inversion wind can explain the "unexpected" location of the maximum in inversion strength. It seems that the nature of the surface winds and the directional constancy are highly comparable between the sloping surfaces of Antarctica and Greenland (van den Broeke et al., 1994; King and Turner, 1997) and in both cases the maximum inversion occurs at non-zero wind speeds.

4.3 Impact from clouds

The difference in LW_d radiation between clear-sky and overcast conditions can result in large differences in both T2m and Tskin due to the cloud effects on the surface radiation budget. As satellite Tskin can only be retrieved during clear-sky conditions, the assessment of the cloud effects on the average conditions is essential to facilitate the combination of satellite and in situ observations. In this section, we therefore assess the inversion strength as a function of the cloud cover and in Sect. 4.3.1 the clear-sky bias is estimated for all sites.

Clear-sky conditions are defined to be cases where CCF<0.3, while overcast conditions are defined to have CCF>0.7. The frequency of clear-sky (overcast) observations is defined as the number of clear-sky (overcast) observations compared to the total number of observations. Figure 9 shows the frequency of clear-sky and overcast observations for each of the observation sites used in this study. The SSC, SICE sites, and EGP all show a much larger frequency of overcast conditions compared to the frequency of clear-sky conditions. The ACC sites show a strong seasonal dependence with more clear-sky observations during summer and more overcast conditions during winter. A similar but much weaker seasonal cycle is seen for UAB. The LAB and SSC sites show limited seasonal variability, while the SICE sites have almost only clear-sky observations from April to July.

The relation between the inversion strength and CCF is shown in Fig 10 for all sites. As expected, the inversion strength decreases with increasing LW_d radiation due to a more extensive cloud cover. The average slope is calculated for each

category: ACC=-0.011±0.0037 °C/%, UAB = -0.019±0.0012 °C/%, LAB = -0.021±0.0016 °C/%, SSC = -0.016±0.0026 °C/%, SICE = -0.017±0.0048 °C/% where the uncertainties are given as 95% confidence intervals.

Figure 11a-b show how the temperature differences at the ACC sites vary as a function of season and local time for clear-sky and overcast conditions, respectively. Clear-sky conditions show the largest stratification with temperature differences up to 2-3°C during winter and night time. Overcast conditions reduce the temperature gradient at all times, with the maximum temperature differences of about 1°C. During summer around noon, overcast conditions usually lead to an unstable stratification of the order of -1°C. An unstable stratification may also occur during clear-sky conditions and large solar insolation. This behaviour is common for all sites included in this study, but the strength of the inversion varies among the different sites

The impact of season and sky conditions on the T2m-Tskin differences is quantified in Table 2. The table summarizes the findings of the dependencies of cloud/clear and summer/winter on the T2m-Tskin difference for all 5 categories. Note that DMI_Q is withheld from the averaging for the SICE sites to avoid systematic impacts from the 1 m height observations. The categories which experience summer surface melt (UAB + ACC) tend to have larger T2m-Tskin differences during summer than winter. The SSC sites also experience melt, but the snow melts away in summer, which limits the time where Tskin is constrained to the melting point. It is difficult to interpret the results for the SICE sites, as none of the individual sites cover an entire year. For all surface types and for all times of the year, cloud cover tends to decrease the inversion strength.

4.3.1 Clear-sky bias

The most accurate surface temperature satellite observations are thermal IR observations that can only be observed during clear-sky conditions. As the satellite IR observations thus have gaps in cloudy conditions, the satellite Tskin products are often averages of the available satellite observations within 1-3 days (see e.g. Rasmussen et al., 2018). However, these satellite averages can be colder than the all-sky average temperature due to a clear-sky bias arising from the fact that Tskin is typically colder in clear-sky conditions compared to the cloudy conditions where the satellite cannot observe. When using the averaged Tskin observations for monitoring or in combination with ocean, sea ice or atmospheric models, it is therefore important to assess the impact on the clear-sky bias, by using different temporal averaging windows. Hall et al. (2012) show monthly temperature maps from MODIS and discuss the fact that the monthly average temperatures (from satellites) are likely lower that the all-sky monthly average temperatures. Here, we use the in situ observations to estimate the clear-sky effects that satellite observations would introduce. We use the cloud mask derived from the longwave-equivalent cloud cover fraction and assume that it is equivalent to the cloud masks used for IR satellite processing. The clear-sky bias has been assessed by comparing clear-sky Tskin observations with all-sky Tskin (where clear-sky has been defined as a CCF < 0.3) observations, averaged for different time windows: 24 h, 72 h and 1 month, for all sites. The results are shown in Fig. 12. For most stations all-sky observations are warmer than clear-sky observations for all time windows. However, there is large

variability among the stations and at a few stations e.g. EGP, KPC_U, ATQ, OLI and DMI_Q the all-sky observations are colder than clear-sky observations using one or more of the time windows.

The larger clear sky biases for longer temporal averaging windows arise from persistent cloud cover lasting for days. For e.g. the 72 hours temporal averaging intervals, observations from periods with >1 day persistent cloud cover (and higher Tskin) are included, which are otherwise missing in the 24 hour clear-sky averages, resulting in a warmer all-sky averaged Tskin, compared to the average clear-sky Tskin.

Figure 13 shows the monthly mean difference in 24 h averaged clear-sky and all-sky Tskin for the ACC stations (a) and the LAB stations (b). For both groups of stations it is found that the 24 h averaged clear-sky bias is closest to zero during summer, which can partly be explained by the smaller daily Tskin range in summer (Fig. 5b). The UAB sites look very similar to the LAB sites, but with a slightly more pronounced seasonal cycle in the clear-sky bias. The figures have not been produced for the SSC and SICE sites as none of the individual sites included in these categories cover an entire season. The orange graphs show the mean number of hours with clear-sky per day, which illustrate more hours with clear-skies for LAB stations compared to ACC stations except for May-July. The positive clears-sky biases observed in Fig. 12 are very likely an effect of seasonal differences in cloud cover e.g. it is found that EGP has no clear-sky observations in Dec.-Feb. and at DMI_Q there is no clear-sky observations available Jan-Mar., which means that the results in Fig. 12 is biased towards the months where a zero or positive clear-sky bias is observed. The 72 h and 1 month averaged clear-sky biases show the same seasonal variation as in Fig. 13, with the smallest biases in summer and largest biases in winter.

4.4 Relationship with skin surface temperature

Section 4.3 showed how clouds impact the T2m and Tskin relationship, and Sect. 4.3.1 revealed a close relationship between Tskin and the CCF. With the aim of deriving T2m based upon satellite Tskin observations, it is important to examine how the T2m-Tskin difference is related to the skin temperature itself. The relationship with Tskin is corroborated in Fig. 14 where the strength of the surface-based inversion is shown as a function of Tskin. All PROMICE sites show an almost linear trend towards weaker inversion strength for higher skin temperatures with the steepest slope of the curve for low elevation sites. The average slopes for all categories are found to: ACC=-0.030±0.003, UAB =-0.066±0.004, LAB=-0.101±0.004, SSC = -0.044±0.005, SICE = -0.043±0.007, where the uncertainty estimates are given as 95 % confidence intervals. The results of this section are very encouraging in a situation where we would like to relate Tskin to T2m, but the cloud cover and longwave radiation are not available, such as the case with satellite observations.

5 Discussion

The T2m and Tskin variability shows that the coldest month ranges from December to March, whereas the warmest month is July for all sites considering both Tskin and T2m. This is in agreement with mean air temperatures found in Steffen and Box (2001) for Greenland GC-Net AWSs, Persson (2002) for Arctic sea ice and Rigor et al. (2000) for North Pole stations and

land stations in Alaska. The monthly mean daily temperature range is largest in April-May and reaches a minimum in July, related to the upper temperature limit when the ice or snow is melting. Surface temperature inversions are very common for the Arctic region. Considering all categories the mean temperature difference between T2m and Tskin is on average 0.65-2.65°C with the strongest inversion for the sites located in the lower part of the ablation zone and the weakest inversion for the sea ice sites. Inversions are predominantly found during winter (low-sun and polar night periods), which allows for a strong radiative cooling at the surface. Smaller temperature differences are dominating in spring and summer, around noon and early afternoon, where the sun is warming the surface. This is in agreement with Adolph et al. (2018) who found large T2m-Tskin differences during night time and small differences during the peak solar irradiance (see Fig. 5 in Adolph et al., 2018). During summer and local noon Tskin has the closest coupling to T2m and the satellite observed Tskin observations will therefore have the best agreement with the T2m at these times.

Increasing wind speeds are expected to decrease the inversion strength through increased turbulence, and mixing warmer air downwards. This is also seen at the ARM sites and Arctic sea ice sites, where the strongest inversion occurs at calm winds and weaker inversions occur with increasing wind speed. The relationship is more complicated over a sloping terrain with the maximum inversion strength at winds of about 5 m s^{-1} and not at calm winds. This feature has previously been identified by others for Antarctica (Hudson and Brandt, 2005) and at Summit, GrIS (Adolph et al., 2018; Miller et al., 2013) and can be explained by the presence of a katabatic wind driven by the surface temperature inversion over a sloping terrain. The katabatic wind destroys part of its own forcing and as a result there exist an optimum in inversion strength and wind speed. This is in agreement with what Hudson and Brandt (2005) found for the Antarctic ice sheet.

The analysis of the impact of clouds showed an almost linear relationship between cloud cover and the T2m-Tskin difference, with a trend towards zero with increasing CCF (Fig. 10). Considering all categories the T2m-Tskin difference decreases from an all-sky mean value ranging from 0.65-2.65°C to a difference ranging from -0.08-1.63°C considering observations with a CCF above 0.7. On the other hand, the difference increases to the range of 1.05-3.44°C by only considering observations with CCFs below 0.3. The smaller inversion strength under cloudy conditions is explained by the fact that clouds have a predominantly warming effect on the surface in the Arctic (Intrieri, 2002; Walsh and Chapman, 1998). In cases where the cloud cover and longwave radiation are not available, the relationship can be quantified by using the Tskin. We have found an almost linear relationship between the inversion strength and the skin temperatures, with weaker inversions for higher Tskin. This is in agreement with Adolph et al. (2018) who found larger T2m-Tskin differences at lower temperatures at the Summit station, during summer.

As mentioned earlier, the measurement height changes with snowfall and snow melt at with that the strength of the inversion measured. The PROMICE data includes a height of the sensor boom, which can be used to determine the impact of using different measurement height on our results. We reproduced the numbers in Table 2, based upon observations measured at a height of 1.9-2.1 m only and found overall all-sky, all-months differences less than 0.22°C for all the different PROMICE regions. In addition, the screening did not change the conclusions regarding the impact of clouds and the seasonal behaviour of the T2m-Tskin differences. Data from the other sites do not all include such information on the measurement height. For

consistency, we therefore chose not to screen the PROMICE data. In addition, we chose not to perform an adjustment of the observations, as we estimate the uncertainty of such an adjustment to be equal to or larger than the actual uncertainty on the results obtained here and again, it would not be possible to make such a correction for all sites.

To assess if there is any impact of clear-sky observations on the radiometer observations due to the different spectral characteristics (broad band versus narrow band, as discussed in Sect. 2.7), the T2m-Tskin differences as a function of CCF were calculated for narrow band Tskin and broad band Tskin for the stations containing both instruments (ATQ, BAR, OLI, DMI_Q, SHEBA, and FRAM). This resulted in a small change in the slope from -0.017 to 0.020°C/% for narrow band and broad band Tskin estimates, respectively. Similarly, the T2m-Tskin differences were calculated for both types of radiometers as a function of Tskin. Again, the change in trend was small from -0.046 to -0.055.

The influence of clouds on Tskin has been assessed by comparing clear-sky Tskin observations with all-sky Tskin observations averaged for different time intervals: 24 h, 72 h and 1 month, for all sites. In general, the clear-sky average is colder than the all-sky average with increasing bias with the length of the averaging time interval and the clear-sky bias is smaller during summer than winter for all averaging windows. This is also reported by Comiso (2000), who finds a monthly mean clear-sky bias of about -0.3°C during summer (Jan.) and -0.5°C during winter (Jul.) at Antarctic stations. The range in temperature over the averaging window as well as the frequency and timing of clear-sky observations are factors partly explaining the clear-sky bias variations observed among the stations.

The observed clear-sky bias explains part of the cold bias observed in IR satellite retrievals of skin surface temperature compared to in situ surface temperatures (Høyer et al., 2017; Rasmussen et al., 2018; Shuman et al., 2014). Another part of the explanation is related to the fact that the satellite skin observations are compared to in situ measured at typically 2 m height, where the temperature gradients in the lowest 2 m of the atmosphere will result in the satellite retrievals of surface temperature being colder than the in situ measurements at 2 m height.

6 Conclusions

Coincident in situ skin temperature (Tskin) and 2 m air temperatures (T2m) from 29 deployments in the Arctic region have been analysed to assess the variability and the factors controlling the Tskin and T2m variations in order to facilitate the combined use of satellite observed Tskin and traditional observations of T2m. The extensive data set used in this study represents a wide range of conditions including all-year observations from Arctic sea ice, land ice in northern Alaska as well as low and high altitude land ice covering the lower, middle and upper ablation zones and the accumulation region of the Greenland Ice Sheet. It has been found that there is a good correspondence between the Tskin and T2m and that the main factors influencing the relationship are seasonal variations, wind speed, cloud cover and the Tskin of the surface. The assessment of the tight relationship and the identification of the main variables that controls the variability are important findings when developing a statistical model that can convert satellite Tskin observations to T2m. All the identified parameters can be derived from either the satellite retrievals themselves or from NWP analysis and the generation of a daily

satellite derived T2m product for the Polar Regions is thus made possible with these results. Such a satellite derived product will be independent of other existing surface temperature products and NWP reanalysis and can therefore contribute significantly to improvements in the Arctic climate change assessment since the satellite era started in the early 1980'ies.

7 Author contribution

Pia Nielsen-Englyst, Kristine S. Madsen, Rasmus Tonboe, Gorm Dybkjær and Emy Alerskans compiled the in situ data. Pia Nielsen-Englyst, Jacob L. Høyer and Kristine S. Madsen designed the experiments and Pia Nielsen-Englyst carried them out. Pia Nielsen-Englyst prepared the manuscript with contributions from all authors.

8 Competing interests

The authors declare that they have no conflict of interest.

9 Acknowledgements

This study was carried out as a part of the European Union Surface Temperatures for All Corners of Earth (EUSTACE), which is financed by the European Union's Horizon 2020 Programme for Research and Innovation, under Grant Agreement no 640171. The aim of EUSTACE is to provide a spatially complete daily field of air temperatures since 1850 by combining satellite and in situ observations. The author would like to thank the data providers. Data was provided by PROMICE, which is funded by the Danish Ministry of Climate, Energy and Building, operated by the Geological Survey of Denmark and Greenland and conducted in collaboration with the National Space Institute (DTU Space) and Asiaq (Greenland Survey) at http://www.promice.dk. Data were also obtained from the Atmospheric Radiation Measurement (ARM) Climate Research Facility, a U.S. Department of Energy Office of Science user facility sponsored by the Office of Biological and Environmental Research. We thank our colleagues in the SHEBA Atmospheric Surface Flux Group, Ed Andreas, Chris Fairall, Peter Guest, and Ola Persson for help collecting and processing the data. The National Science Foundation supported this research with grants to the U.S. Army Cold Regions Research and Engineering Laboratory, NOAA's Environmental Technology Laboratory, and the Naval Postgraduate School. Data was also provided by Timo Palo from the Tara expedition, supported by the European Commission 6th Framework Integrated Project DAMOCLES and in part by the Academy of Finland through the CACSI project. We thank Steinar Eastwood from the Norwegian Meteorological Institute for providing us with data from the FRAM2014/15 expedition. Finally, we would like to thank the anonymous reviewers for their carefully reading and their insightful suggestions and comments, which substantially improved this manuscript.

References

Abermann, J., Hansen, B., Lund, M., Wacker, S., Karami, M. and Cappelen, J.: Hotspots and key periods of Greenland climate change during the past six decades, Ambio, 46(S1), 3–11, doi:10.1007/s13280-016-0861-y, 2017.

Ackerman, T. P. and Stokes, G. M.: The Atmospheric Radiation Measurement Program, Phys. Today, 56(1), 38–44, doi:10.1063/1.1554135, 2003.

Adolph, A. C., Albert, M. R. and Hall, D. K.: Near-surface temperature inversion during summer at Summit, Greenland, and its relation to MODIS-derived surface temperatures, The Cryosphere, 12(3), 907–920, doi:10.5194/tc-12-907-2018, 2018.

Ahlstrøm, A., van As, D., Citterio, M., Andersen, S., Fausto, R., Andersen, M., Forsberg, R., Stenseng, L., Lintz Christensen, E. and Kristensen, S. S.: A new Programme for Monitoring the Mass Loss of the Greenland Ice Sheet, Geol. Surv. Den. Greenl. Bull., 15, 61–64, 2008.

Box, J. E., Fettweis, X., Stroeve, J. C., Tedesco, M., Hall, D. K. and Steffen, K.: Greenland ice sheet albedo feedback: thermodynamics and atmospheric drivers, The Cryosphere, 6(4), 821–839, doi:10.5194/tc-6-821-2012, 2012.

Bretherton, C. S., Roode, S. R. de, Jakob, C., Andreas, E. L., Intrieri, J., Moritz, R. E. and Persson, O. G.: A comparison of the ECMWF forecast model with observations over the annual cycle at SHEBA. Unpublished manuscript, 2000.

Cappelen, J.: Greenland—DMI Historical Climate Data Collection 1784–2015. Danish Meteorological Institute., 2016.

Casey, K. A., Polashenski, C. M., Chen, J. and Tedesco, M.: Impact of MODIS sensor calibration updates on Greenland Ice Sheet surface reflectance and albedo trends, The Cryosphere, 11(4), 1781–1795, doi:10.5194/tc-11-1781-2017, 2017.

Cohen, J., Screen, J. A., Furtado, J. C., Barlow, M., Whittleston, D., Coumou, D., Francis, J., Dethloff, K., Entekhabi, D., Overland, J. and Jones, J.: Recent Arctic amplification and extreme mid-latitude weather, Nat. Geosci., 7(9), 627–637, doi:10.1038/ngeo2234, 2014.

Comiso, J. C.: Variability and Trends in Antarctic Surface Temperatures from In Situ and Satellite Infrared Measurements, J. Clim., 13(10), 1674–1696, doi:10.1175/1520-0442(2000)013<1674:VATIAS>2.0.CO;2, 2000.

Curry, J. A. and Herman, G. F.: Infrared Radiative Properties of Summertime Arctic Stratus Clouds, J. Clim. Appl. Meteorol., 24(6), 525–538, doi:10.1175/1520-0450(1985)024<0525:IRPOSA>2.0.CO;2, 1985.

Curry, J. A., Schramm, J. L., Rossow, W. B. and Randall, D.: Overview of Arctic Cloud and Radiation Characteristics, J. Clim., 9(8), 1731–1764, doi:10.1175/1520-0442(1996)009<1731:OOACAR>2.0.CO;2, 1996.

Dozier, J. and Warren, S. G.: Effect of viewing angle on the infrared brightness temperature of snow, Water Resour. Res., 18(5), 1424–1434, doi:10.1029/WR018i005p01424, 1982.

Dybkjær, G., Tonboe, R. and Høyer, J. L.: Arctic surface temperatures from MetOp AVHRR compared to in situ ocean and land data, Ocean Sci., 8(6), 959–970, doi:10.5194/os-8-959-2012, 2012.

Franco, B., Fettweis, X. and Erpicum, M.: Future projections of the Greenland ice sheet energy balance driving the surface melt, The Cryosphere, 7(1), 1–18, doi:10.5194/tc-7-1-2013, 2013.

Gascard, J.-C., Festy, J., le Goff, H., Weber, M., Bruemmer, B., Offermann, M., Doble, M., Wadhams, P., Forsberg, R., Hanson, S., Skourup, H., Gerland, S., Nicolaus, M., Metaxian, J.-P., Grangeon, J., Haapala, J., Rinne, E., Haas, C., Wegener, A., Heygster, G., Jakobson, E., Palo, T., Wilkinson, J., Kaleschke, L., Claffey, K., Elder, B. and Bottenheim, J.: Exploring Arctic Transpolar Drift During Dramatic Sea Ice Retreat, Eos Trans. Am. Geophys. Union, 89(3), 21, doi:10.1029/2008EO030001, 2008.

Good, E. J., Ghent, D. J., Bulgin, C. E. and Remedios, J. J.: A spatiotemporal analysis of the relationship between near-surface air temperature and satellite land surface temperatures using 17 years of data from the ATSR series, J. Geophys. Res. Atmospheres, 122(17), 9185–9210, doi:10.1002/2017JD026880, 2017.

Graversen, R. G., Mauritsen, T., Tjernström, M., Källén, E. and Svensson, G.: Vertical structure of recent Arctic warming, Nature, 451(7174), 53–56, doi:10.1038/nature06502, 2008.

Hall, D., Box, J., Casey, K., Hook, S., Shuman, C. and Steffen, K.: Comparison of satellite-derived and in-situ observations of ice and snow surface temperatures over Greenland, Remote Sens. Environ., 112(10), 3739–3749, doi:10.1016/j.rse.2008.05.007, 2008.

Hall, D. K., Comiso, J. C., DiGirolamo, N. E., Shuman, C. A., Key, J. R. and Koenig, L. S.: A Satellite-Derived Climate-Quality Data Record of the Clear-Sky Surface Temperature of the Greenland Ice Sheet, J. Clim., 25(14), 4785–4798, doi:10.1175/JCLI-D-11-00365.1, 2012.

Hansen, J., Ruedy, R., Sato, M. and Lo, K.: Global surface temperature change, Rev. Geophys., 48(4), doi:10.1029/2010RG000345, 2010.

Høyer, J. L., Lang, A. M., Tonboe, R., Eastwood, S., Wimmer, W. and Dybkjær, G.: Towards field inter-comparison experiment (FICE) for ice surface temperature (ESA Tech. Rep. FRM4STS OP-40)., [online] Available from: http://www.frm4sts.org/wp-content/uploads/sites/3/2017/12/OFE-OP-40-TR-5-V1-Iss-1-Ver-1-Signed.pdf, 2017.

Hudson, S. R. and Brandt, R. E.: A Look at the Surface-Based Temperature Inversion on the Antarctic Plateau, J. Clim., 18(11), 1673–1696, doi:10.1175/JCLI3360.1, 2005.

Intrieri, J. M.: An annual cycle of Arctic surface cloud forcing at SHEBA, J. Geophys. Res., 107(C10), doi:10.1029/2000JC000439, 2002.

Jones, P. D., Lister, D. H., Osborn, T. J., Harpham, C., Salmon, M. and Morice, C. P.: Hemispheric and large-scale land-surface air temperature variations: An extensive revision and an update to 2010:, J. Geophys. Res. Atmospheres, 117(D5), n/a-n/a, doi:10.1029/2011JD017139, 2012.

King, J. C. and Turner, J.: Antarctic Meteorology and Climatology, Cambridge University Press, Cambridge., 1997.

Koenig, L. S. and Hall, D. K.: Comparison of satellite, thermochron and air temperatures at Summit, Greenland, during the winter of 2008/09, J. Glaciol., 56(198), 735–741, doi:10.3189/002214310793146269, 2010.

Kristoffersen, Y. and Hall, J.: Hovercraft as a Mobile Science Platform Over Sea Ice in the Arctic Ocean, Oceanography, 27(2), doi:10.5670/oceanog.2014.33, 2014.

Lettau, H. H. and Schwerdtfeger, W.: Dynamics of the surface-wind regime over the interior of Antarctica, Antarct. J. U. S., 2(5), 155–158, 1967.

Mahrt, L. J. and Schwerdtfeger, W.: Ekman spirals for exponential thermal wind, Bound.-Layer Meteorol., 1(2), 137–145, doi:10.1007/BF00185735, 1970.

Masson-Delmotte, V., Swingedouw, D., Landais, A., Seidenkrantz, M.-S., Gauthier, E., Bichet, V., Massa, C., Perren, B., Jomelli, V., Adalgeirsdottir, G., Hesselbjerg Christensen, J., Arneborg, J., Bhatt, U., Walker, D. A., Elberling, B., Gillet-Chaulet, F., Ritz, C., Gallée, H., van den Broeke, M., Fettweis, X., de Vernal, A. and Vinther, B.: Greenland climate change: from the past to the future: Greenland climate change, Wiley Interdiscip. Rev. Clim. Change, 3(5), 427–449, doi:10.1002/wcc.186, 2012.

Maykut, G. A.: The Surface Heat and Mass Balance, in The Geophysics of Sea Ice, edited by N. Untersteiner, pp. 395–463, Springer US, Boston, MA., 1986.

Miller, N. B., Turner, D. D., Bennartz, R., Shupe, M. D., Kulie, M. S., Cadeddu, M. P. and Walden, V. P.: Surface-based inversions above central Greenland, J. Geophys. Res. Atmospheres, 118(2), 495–506, doi:10.1029/2012JD018867, 2013.

Monin, A. S. and Obukhov, A. M.: Basic Laws of Turbulent Mixing in the Surface Layer of the Atmosphere, Contrib. Geophys. Inst. Slovak Acad. Sci., USSR 151.163, 1954.

Moris, V. R.: Infrared Thermometer (IRT) Handbook Atmospheric Radiation Measurement publication ARM TR-015 available from https://www.arm.gov/instruments/irt, 2006.

Overland, J., Francis, J. A., Hall, R., Hanna, E., Kim, S.-J. and Vihma, T.: The Melting Arctic and Midlatitude Weather Patterns: Are They Connected?*, J. Clim., 28(20), 7917–7932, doi:10.1175/JCLI-D-14-00822.1, 2015.

Persson, P. O. G.: Measurements near the Atmospheric Surface Flux Group tower at SHEBA: Near-surface conditions and surface energy budget, J. Geophys. Res., 107(C10), doi:10.1029/2000JC000705, 2002.

Rasmussen, T. A. S., Høyer, J. L., Ghent, D., Bulgin, C. E., Dybkjaer, G., Ribergaard, M. H., Nielsen-Englyst, P. and Madsen, K. S.: Impact of Assimilation of Sea-Ice Surface Temperatures on a Coupled Ocean and Sea-Ice Model, J. Geophys. Res. Oceans, 123(4), 2440–2460, doi:10.1002/2017JC013481, 2018.

Rayner, N. A.: Global analyses of sea surface temperature, sea ice, and night marine air temperature since the late nineteenth century, J. Geophys. Res., 108(D14), doi:10.1029/2002JD002670, 2003.

Reeves Eyre, J. E. J. and Zeng, X.: Evaluation of Greenland near surface air temperature datasets, The Cryosphere, 11(4), 1591–1605, doi:10.5194/tc-11-1591-2017, 2017.

Rignot, E.: Changes in the Velocity Structure of the Greenland Ice Sheet, Science, 311(5763), 986–990, doi:10.1126/science.1121381, 2006.

Rigor, I. G., Colony, R. L. and Martin, S.: Variations in Surface Air Temperature Observations in the Arctic, 1979–97, J. Clim., 13(5), 896–914, doi:10.1175/1520-0442(2000)013<0896:VISATO>2.0.CO;2, 2000.

Serreze, M. C., Schnell, R. C. and Kahl, J. D.: Low-Level Temperature Inversions of the Eurasian Arctic and Comparisons with Soviet Drifting Station Data, J. Clim., 5(6), 615–629, doi:10.1175/1520-0442(1992)005<0615:LLTIOT>2.0.CO;2, 1992.

Shuman, C. A., Hall, D. K., DiGirolamo, N. E., Mefford, T. K. and Schnaubelt, M. J.: Comparison of Near-Surface Air Temperatures and MODIS Ice-Surface Temperatures at Summit, Greenland (2008–13), J. Appl. Meteorol. Climatol., 53(9), 2171–2180, doi:10.1175/JAMC-D-14-0023.1, 2014.

Stamnes, K., Ellingson, R. G., Curry, J. A., Walsh, J. E. and Zak, B. D.: Review of Science Issues, Deployment Strategy, and Status for the ARM North Slope of Alaska–Adjacent Arctic Ocean Climate Research Site, J. Clim., 12(1), 46–63, doi:10.1175/1520-0442-12.1.46, 1999.

Steffen, K.: Surface energy exchange at the equilibrium line on the Greenland ice sheet during onset of melt, Ann. Glaciol., 21, 13–18, doi:10.3189/S0260305500015536, 1995.

Steffen, K. and Box, J.: Surface climatology of the Greenland Ice Sheet: Greenland Climate Network 1995-1999, J. Geophys. Res. Atmospheres, 106(D24), 33951–33964, doi:10.1029/2001JD900161, 2001.

Stocker, T. F., Qin, D., Plattner, G.-K., Tignor, M., Allen, S. K., Boschung, J., Nauels, A., Xia, Y., Bex, V., Midgley, P. M. and (eds.): Climate Change 2013 - The Physical Science Basis: Working Group I Contribution to the Fifth Assessment Report of the Intergovernmental Panel on Climate Change, Cambridge University Press, Cambridge., 2014.

Stroeve, J., Box, J. E., Wang, Z., Schaaf, C. and Barrett, A.: Re-evaluation of MODIS MCD43 Greenland albedo accuracy and trends, Remote Sens. Environ., 138, 199–214, doi:10.1016/j.rse.2013.07.023, 2013.

Swinbank, W. C.: Long-wave radiation from clear skies, Q. J. R. Meteorol. Soc., 89(381), 339–348, doi:10.1002/qj.49708938105, 1963.

Tedesco, M., Fettweis, X., van den Broeke, M. R., van de Wal, R. S. W., Smeets, C. J. P. P., van de Berg, W. J., Serreze, M. C. and Box, J. E.: The role of albedo and accumulation in the 2010 melting record in Greenland, Environ. Res. Lett., 6(1), 014005, doi:10.1088/1748-9326/6/1/014005, 2011.

Uttal, T., Curry, J. A., Mcphee, M. G., Perovich, D. K., Moritz, R. E., Maslanik, J. A., Guest, P. S., Stern, H. L., Moore, J. A., Turenne, R., Heiberg, A., Serreze, M. C., Wylie, D. P., Persson, O. G., Paulson, C. A., Halle, C., Morison, J. H., Wheeler, P. A., Makshtas, A., Welch, H., Shupe, M. D., Intrieri, J. M., Stamnes, K., Lindsey, R. W., Pinkel, R., Pegau, W. S., Stanton, T. P. and Grenfeld, T. C.: Surface Heat Budget of the Arctic Ocean, Bull. Am. Meteorol. Soc., 83(2), 255–275, doi:10.1175/1520-0477(2002)083<0255:SHBOTA>2.3.CO;2, 2002.

van As, D.: Warming, glacier melt and surface energy budget from weather station observations in the Melville Bay region of northwest Greenland, J. Glaciol., 57(202), 208–220, doi:10.3189/002214311796405898, 2011.

van As, D., Broeke, M. van den, Reijmer, C. and Wal, R. van de: The Summer Surface Energy Balance of the High Antarctic Plateau, Bound.-Layer Meteorol., 115(2), 289–317, doi:10.1007/s10546-004-4631-1, 2005.

van As, D., Fausto, R., Steffen, K., Ahlstrøm, A., Andersen, S. B., Andersen, M. L., Box, J., Charalampidis, C., Citterio, M., Colgan, W. T., Edelvang, K., Larsen, S. H., Nielsen, S., Martin, V. and Weidick, A.: Katabatic winds and piteraq storms: Observations from the Greenland ice sheet, Geol. Surv. Den. Greenl. Bull., (31), 83–86, 2014.

van den Broeke, M., Duynkerke, P. and Oerlemans, J.: The observed katabatic flow at the edge of the Greenland ice sheet during GIMEX-91, Glob. Planet. Change, 9(1–2), 3–15, doi:10.1016/0921-8181(94)90003-5, 1994.

Vihma, T.: Effects of Arctic Sea Ice Decline on Weather and Climate: A Review, Surv. Geophys., 35(5), 1175–1214, doi:10.1007/s10712-014-9284-0, 2014.

Vihma, T. and Pirazzini, R.: On the Factors Controlling the Snow Surface and 2-m Air Temperatures Over the Arctic Sea Ice in Winter, Bound.-Layer Meteorol., 117(1), 73–90, doi:10.1007/s10546-004-5938-7, 2005.

Vihma, T., Jaagus, J., Jakobson, E. and Palo, T.: Meteorological conditions in the Arctic Ocean in spring and summer 2007 as recorded on the drifting ice station Tara, Geophys. Res. Lett., 35(18), doi:10.1029/2008GL034681, 2008.

Walsh, J. E.: Intensified warming of the Arctic: Causes and impacts on middle latitudes, Glob. Planet. Change, 117, 52–63, doi:10.1016/j.gloplacha.2014.03.003, 2014.

Walsh, J. E. and Chapman, W. L.: Arctic Cloud–Radiation–Temperature Associations in Observational Data and Atmospheric Reanalyses, J. Clim., 11(11), 3030–3045, doi:10.1175/1520-0442(1998)011<3030:ACRTAI>2.0.CO;2, 1998.

Zhang, Y., Seidel, D. J., Golaz, J.-C., Deser, C. and Tomas, R. A.: Climatological Characteristics of Arctic and Antarctic Surface-Based Inversions, J. Clim., 24(19), 5167–5186, doi:10.1175/2011JCLI4004.1, 2011.

Zygmuntowska, M., Mauritsen, T., Quaas, J. and Kaleschke, L.: Arctic Clouds and Surface Radiation – a critical comparison of satellite retrievals and the ERA-Interim reanalysis, Atmospheric Chem. Phys., 12(14), 6667–6677, doi:10.5194/acp-12-6667-2012, 2012.

5

Table 1 Observation sites used in this study covering the following surface types: Accumulation zone (ACC), upper/middle ablation zone (UAB), lower ablation zone (LAB), seasonal snow cover (SSC), sea ice (SICE).

Project	Site	Station	Surface Type	Latitude (°N)	Longitude (°W)	Elevation (m)	Start date	End date
PROMICE	East Grip	EGP	ACC	75.62	35.97	2660	01/05/2016	30/04/2018
PROMICE	Kangerlussuaq	KAN_U	ACC	67.00	47.03	1840	04/04/2009	03/04/2018
PROMICE	Crown Prince Christian Land	KPC_U	ACC	79.83	25.17	870	17/07/2008	16/07/2018
PROMICE	Kangerlussuaq	KAN_M	UAB	67.07	48.84	1270	02/09/2008	01/09/2018
PROMICE	Nuuk	NUK_N	UAB	64.95	49.89	920	25/07/2010	24/07/2014
PROMICE	Nuuk	NUK_U	UAB	64.51	49.27	1120	20/08/2007	19/08/2018
PROMICE	Qassimiut	QAS_A	UAB	61.24	46.73	1000	20/08/2012	19/08/2015
PROMICE	Qassimiut	QAS_M	UAB	61.10	46.83	630	11/08/2016	10/08/2018
PROMICE	Qassimiut	QAS_U	UAB	61.18	46.82	900	07/08/2008	06/08/2018
PROMICE	Scoresbysund	SCO_U	UAB	72.39	27.23	970	21/07/2008	20/07/2018
PROMICE	Tasiilaq	TAS_A	UAB	65.78	38.90	890	28/08/2013	27/08/2018
PROMICE	Tasiilaq	TAS_U	UAB	65.67	38.87	570	11/03/2008	10/03/2015
PROMICE	Thule	THU_U	UAB	76.42	68.15	760	09/08/2010	08/08/2018
PROMICE	Upernavik	UPE_U	UAB	72.89	53.58	940	18/08/2009	17/08/2018
PROMICE	Kangerlussuaq	KAN_L	LAB	67.10	49.95	670	01/09/2008	31/08/2018
PROMICE	Crown Prince Christian Land	KPC_L	LAB	79.91	24.08	370	17/07/2008	16/07/2018
PROMICE	Nuuk	NUK_L	LAB	64.48	49.54	530	20/08/2007	19/08/2018
PROMICE	Qassimiut	QAS_L	LAB	61.03	46.85	280	24/08/2007	23/08/2018
PROMICE	Scoresbysund	SCO_L	LAB	72.22	26.82	460	22/07/2008	21/07/2018
PROMICE	Tasiilaq	TAS_L	LAB	65.64	38.90	250	23/08/2007	22/08/2018
PROMICE	Thule	THU_L	LAB	76.40	68.27	570	09/08/2010	08/08/2018
PROMICE	Upernavik	UPE_L	LAB	72.90	54.30	220	17/08/2009	16/08/2018
ARM	Atqasuk	ATQ	SSC	70.47	149.89	2	07/11/2003	06/11/2010

ARM	Barrow	BAR	SSC	71.32	156.62	8	31/10/2003	28/10/2018
ARM	Oliktok Point	OLI	SSC	70.50	157.41	20	18/10/2013	13/10/2018
ICEARC	Qaanaaq	DMI_Q	SICE	77.43	69.14	Sea level	31/01/2015	08/06/2017
FRAM2014/15	Arctic Ocean	FRAM	SICE	82.22-89.35	-180.00-180.00	Sea level	05/09/2014	3/07/2015
SHEBA	Arctic Ocean	SHEBA	SICE	74.62-80.37	143.92-168.15	Sea level	01/11/1997	26/09/1998
TARA	Arctic Ocean	TARA	SICE	71.41-88.54	0.01-148.28	Sea level	01/04/2007	20/09/2007

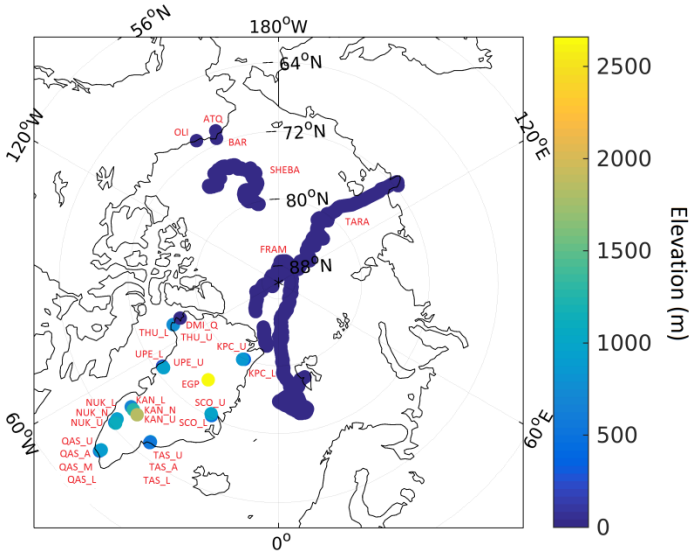

Figure 1: Spatial coverage and elevation for each site included in this study. The colour bar is elevation in meters.

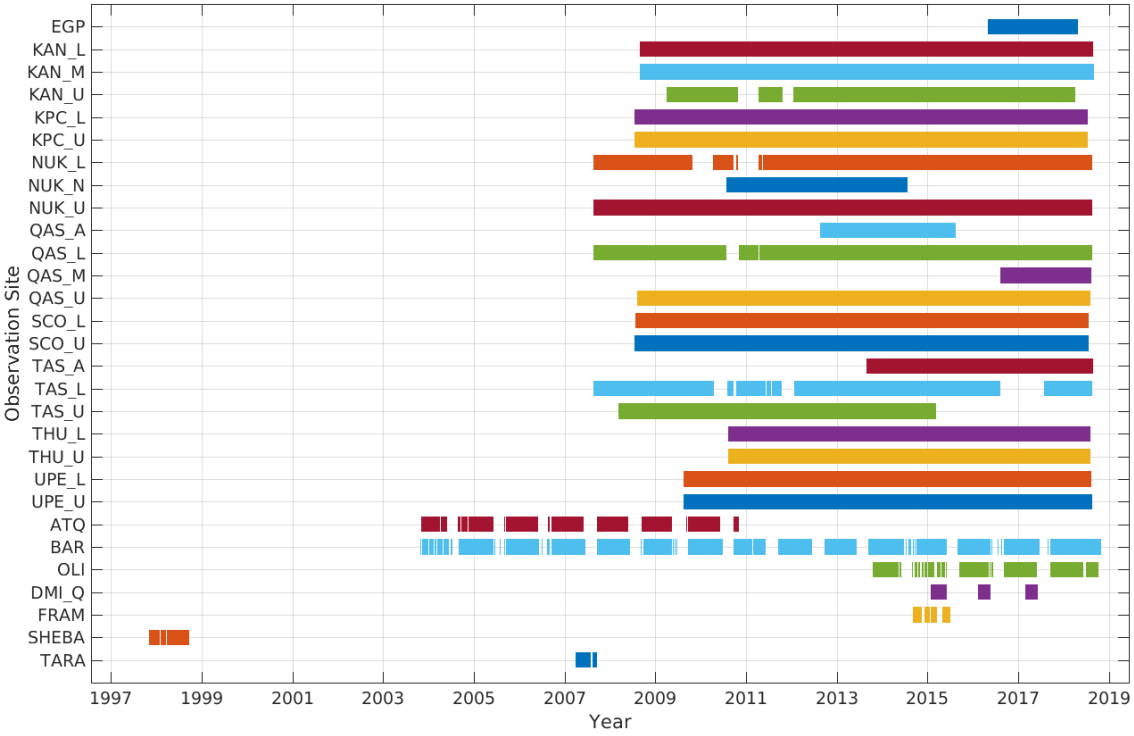

Figure 2: Temporal coverage for each observation site included in this study.

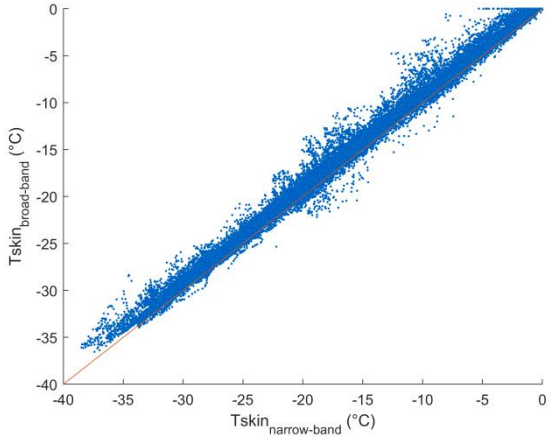

Figure 3: Scatterplot of Tskin estimated from narrow-band IR observations versus Tskin estimated from broad-band IR observations for DMI_Q.

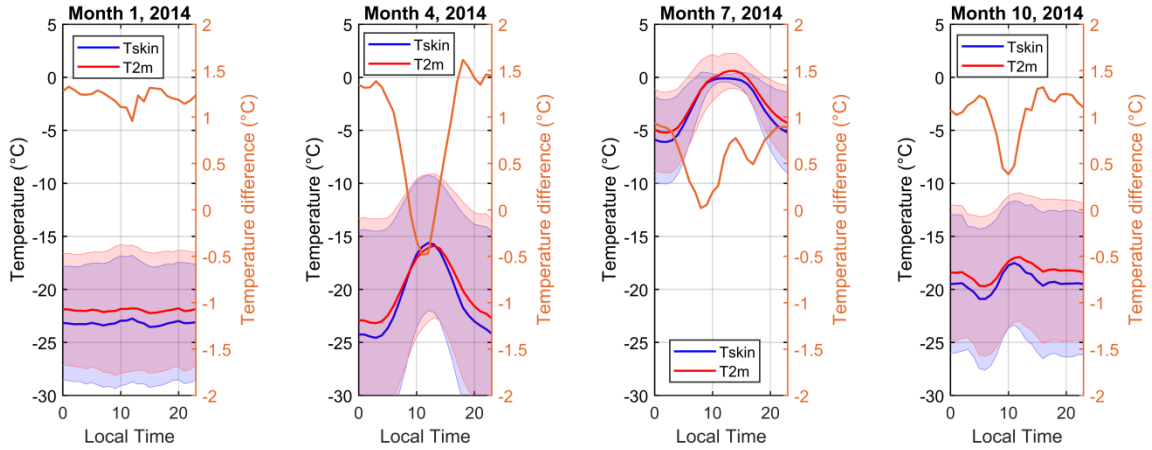

Figure 4: Monthly diurnal variability of 2 m air temperature (red) and skin temperature (blue) at KAN_ U during the months: January, April, July and October. The orange curves are the difference between the red and blue curves. The shadings indicate the standard deviations.

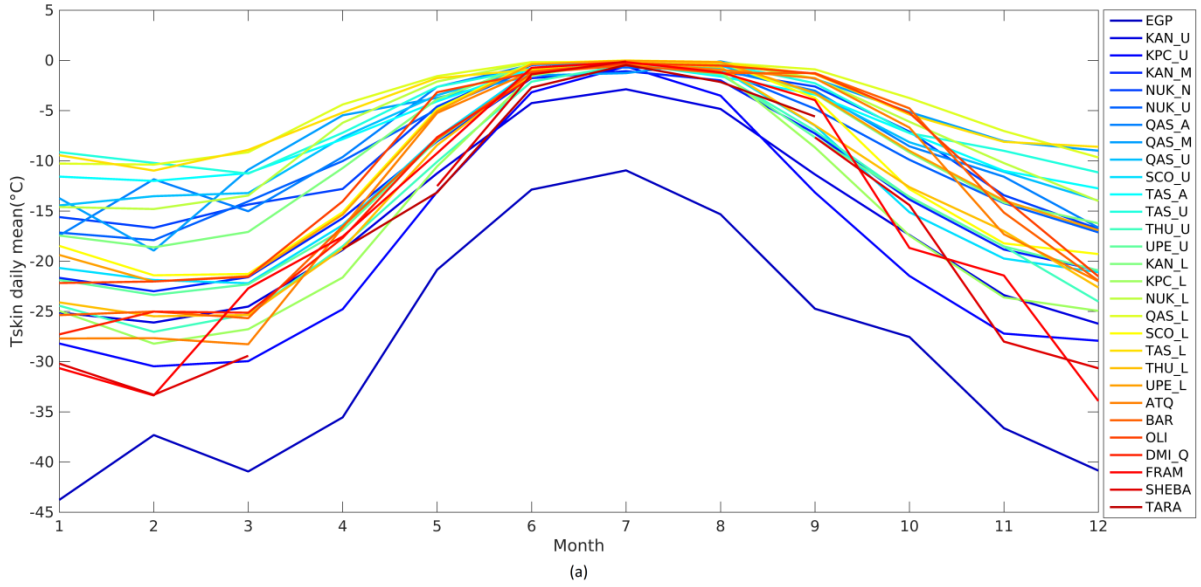

(a)

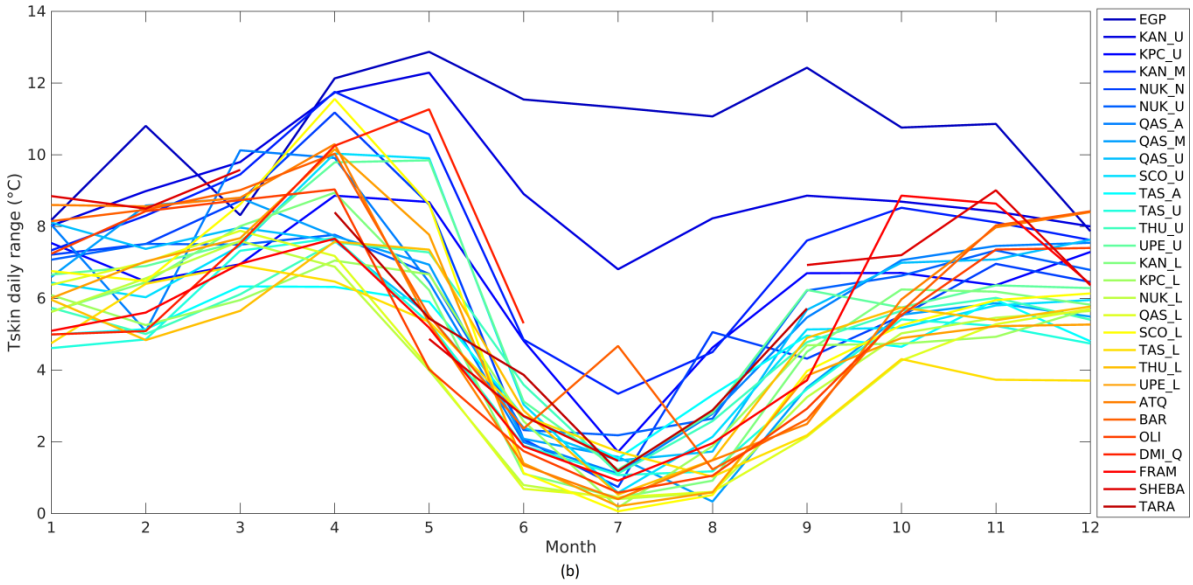

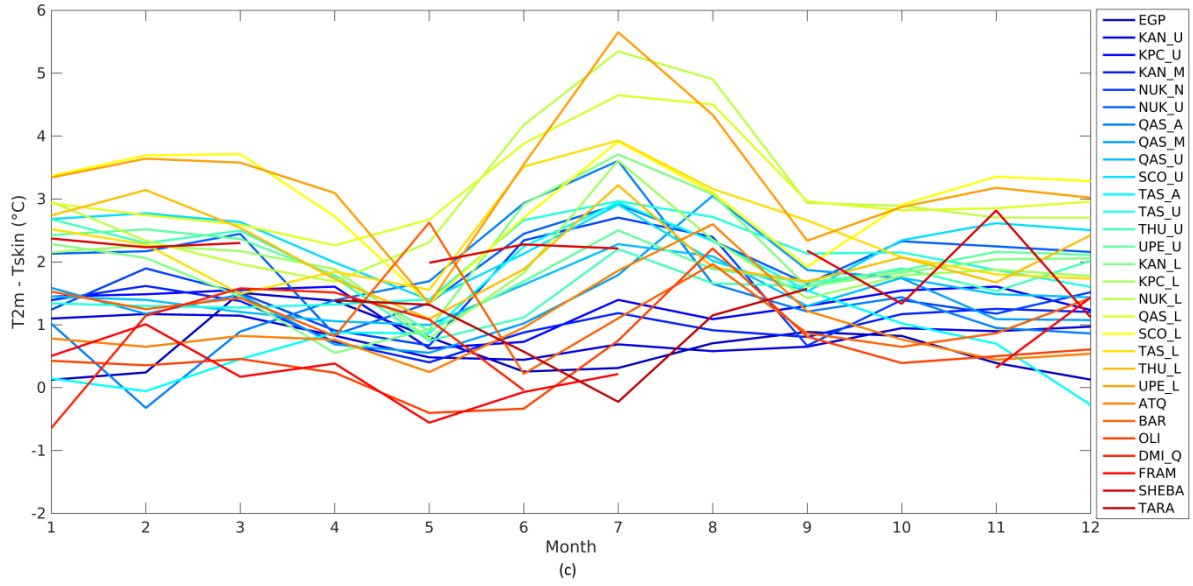

Figure 5: Monthly mean of Tskin (a) daily range in Tskin (b) and T2m-Tskin difference (c), for all sites. See Table 1 for station locations and types.

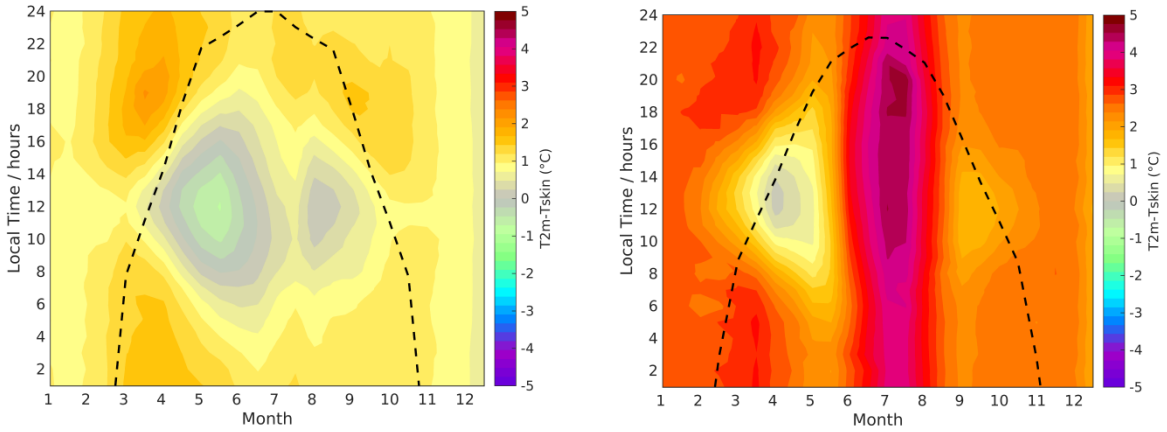

Figure 6: Mean 2 m air temperature and skin temperature differences for ACC (a) and LAB (b) as a function of time of year (with a bin size of 15 days) and local time of the day. The dotted black lines indicate the total hours of sunlight.

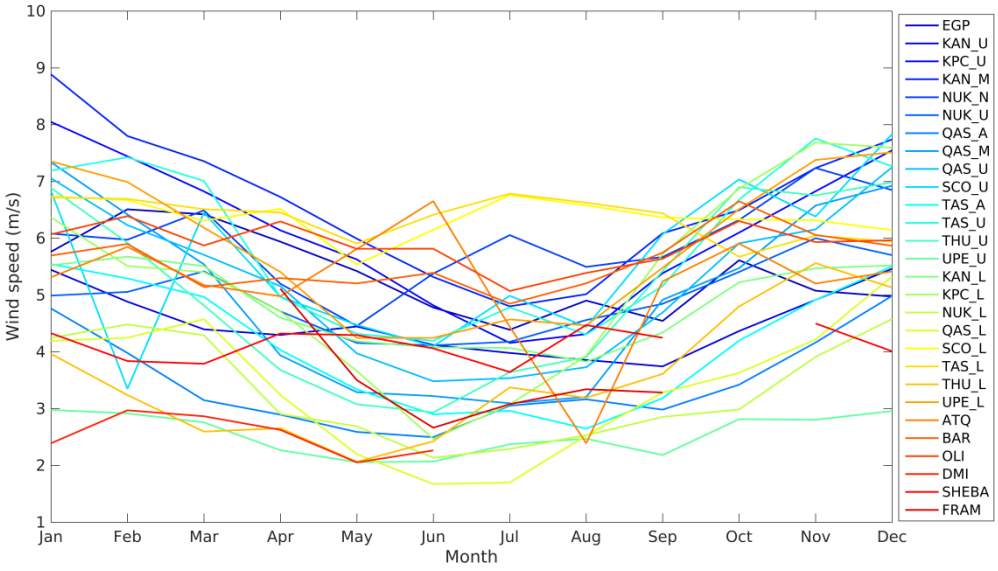

Figure 7: The average annual cycle in wind speed for all sites.

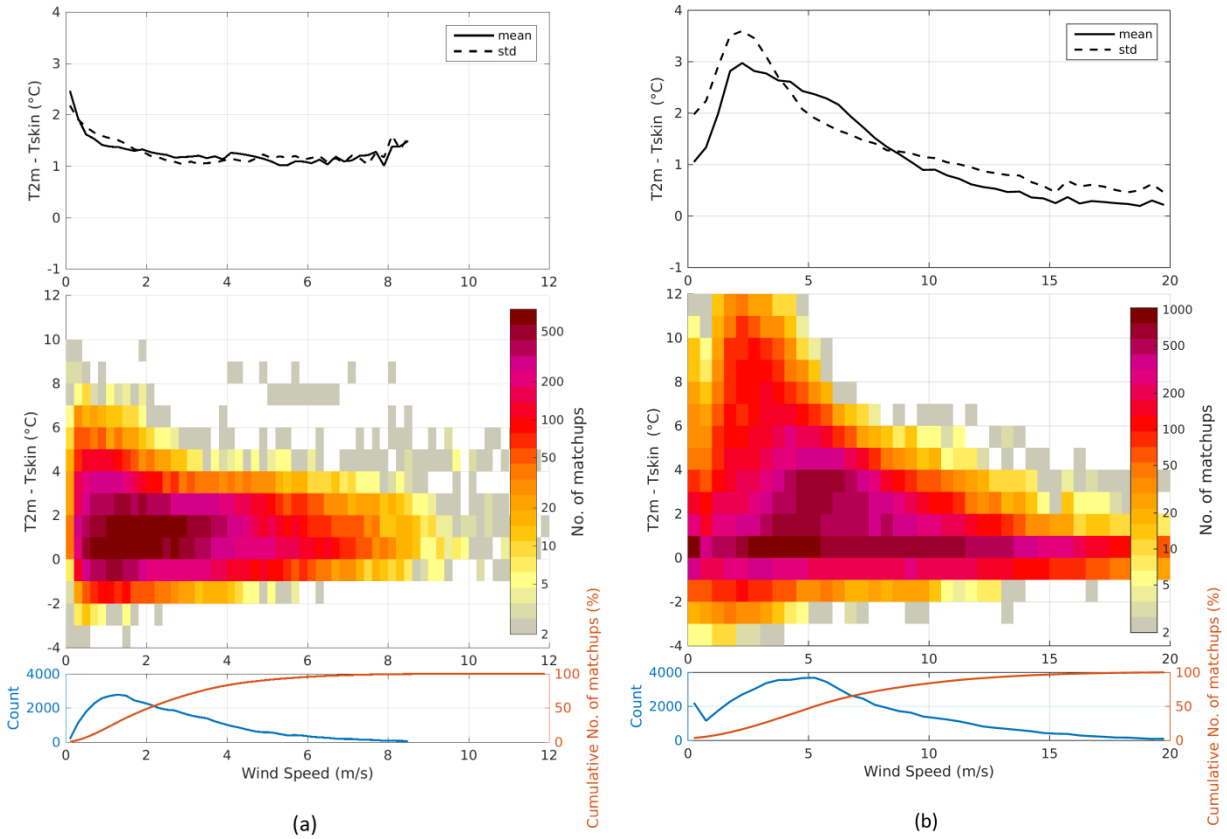

Figure 8: 2 m air temperature and skin temperature difference as a function of binned wind speed for (a) DMI_Q and (b) THU_U. The wind speed bin size is 0.5 m s^{-1}, the T2m-Tskin bin size is 1°C, and only bins with more than 50 members are included. The upper plots show the standard deviation (dashed lines) and mean difference (solid lines). The middle plots show the number of members in each bin, while the bottom plots show the number of members (blue lines) and the cumulative percentage of members (red lines) in each wind speed bin.

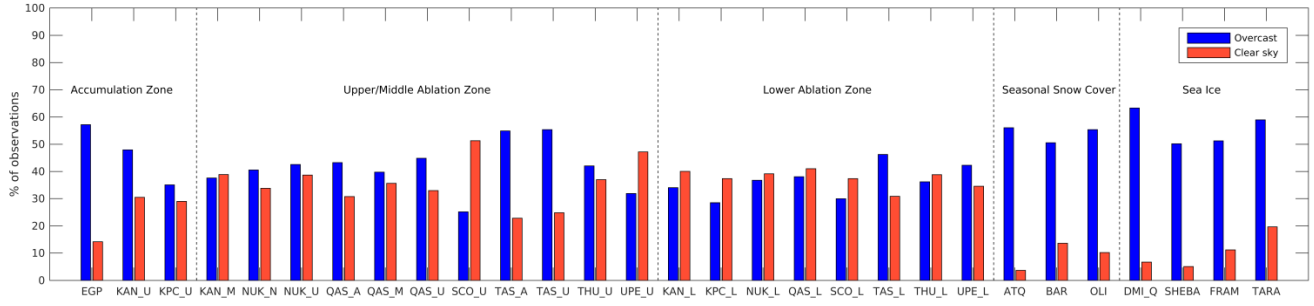

Figure 9: Frequency of clear-sky and overcast observations in percent of all observations for each site.

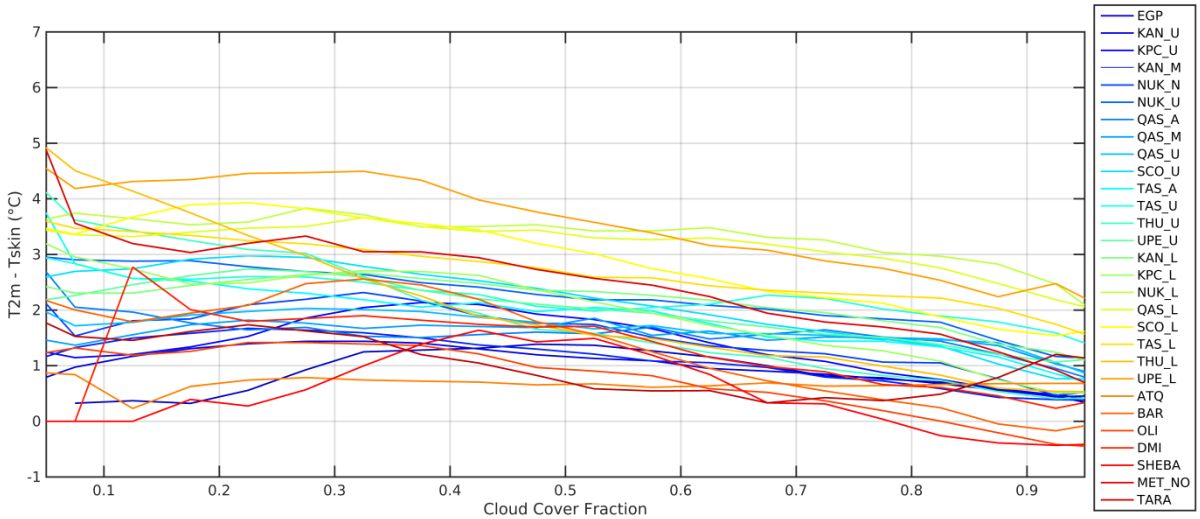

Figure 10: 2 m air temperature and skin temperature differences for all sites as a function of binned cloud cover fraction (CCF). The CCF bin size is 0.05, the T2m-Tskin bin size is 1°C, and only bins with more than 50 members are considered.

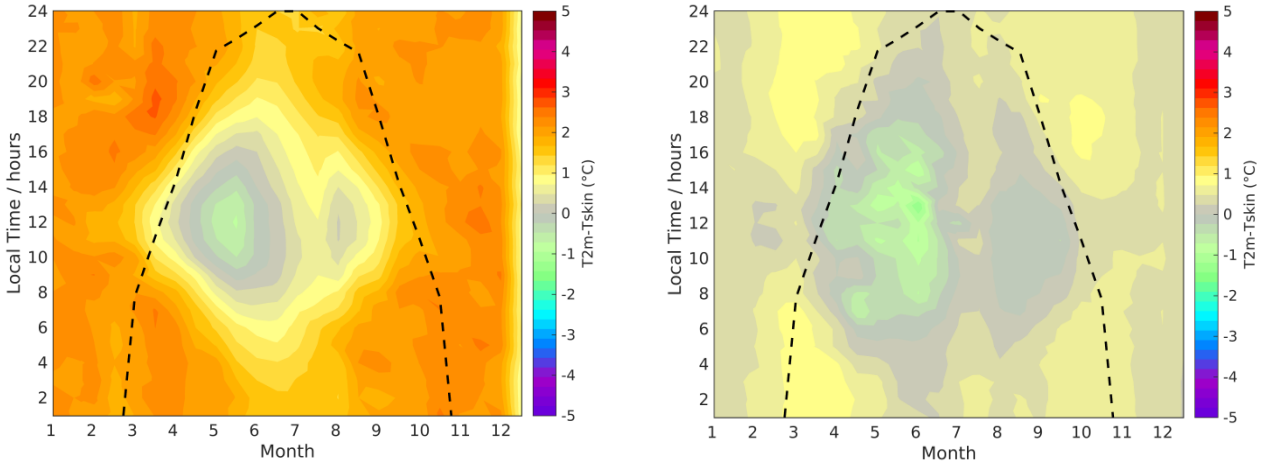

Figure 11: Similar to Fig. 7a but with 2 m air temperature and skin temperature differences for ACC sites in cases of clear-sky (a), and overcast conditions (b). The dotted black lines indicate the total hours of sunlight each month.

Table 2 Overall 2 m air temperature and skin temperature differences (T2m-Tskin, °C) for each surface type under different circumstances in terms of season and sky conditions. The square brackets are the ranges of the T2m-Tskin differences for the stations included in each surface type category.

	Jun-Aug	Dec-Feb	All months

ACC	Cloud	0.21 [0.13 – 0.34]	0.47 [0.16 – 0.66]	0.43 [0.35 – 0.49]
	Clear	0.79 [0.26 – 1.29]	1.99 [1.55 – 2.46]	1.05 [0.58 – 1.50]
	All	0.69 [0.43 – 1.07]	0.88 [0.16 – 1.41]	0.91 [0.65 – 1.29]
UAB	Cloud	1.77 [0.68 – 2.62]	0.67 [-0.79 – 1.52]	0.90 [0.16 – 1.45]
	Clear	2.49 [1.12 – 3.16]	2.71 [1.35 – 4.76]	2.36 [1.45 – 3.38]
	All	2.20 [0.98 – 2.77]	1.60 [0.07 – 2.65]	1.65 [1.05 – 2.26]
LAB	Cloud	2.81 [1.15 – 4.23]	1.38 [0.49 – 2.10]	1.63 [0.66 – 2.41]
	Clear	3.94 [3.01 – 5.22]	3.90 [2.82 – 4.81]	3.44 [2.46 – 4.42]
	All	3.51 [2.28 – 4.74]	2.73 [2.06 – 3.45]	2.65 [1.99 – 3.34]
SSC	Cloud	-0.08 [-0.59 – 0.26]	-0.05 [-0.17 – 0.04]	-0.08 [-0.27 – 0.06]
	Clear	1.57 [1.01 – 2.25]	2.32 [1.75 – 2.93]	1.80 [1.34 – 2.19]
	All	0.40 [-0.22 – 0.96]	0.84 [0.47 – 1.41]	0.65 [0.35 – 0.97]
SICE ÷ DMI_Q	Cloud	0.71 [-0.00 – 1.34]	0.35 [-0.33 – 1.04]	0.64 [-0.38 – 1.29]
	Clear	1.95 [0.40 – 3.73]	2.33 [1.09 – 3.56]	2.10 [0.43 – 3.86]
	All	1.09 [0.08 – 2.30]	1.51 [0.99 – 2.03]	1.25 [0.42 – 2.08]

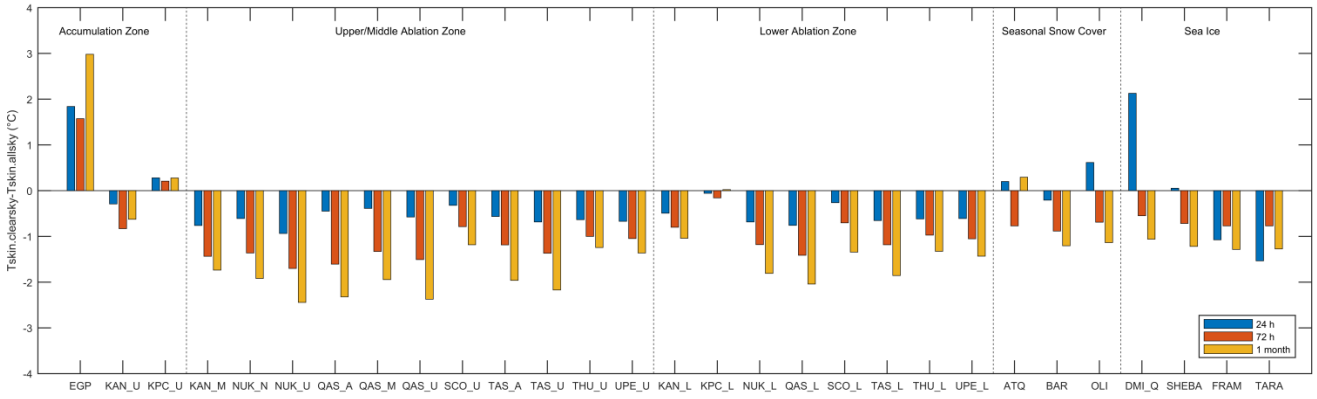

Figure 12: Observed clear-sky biases (Tskin_clearsky-Tskin_allsky) averaged for different time intervals, for all sites (°C).

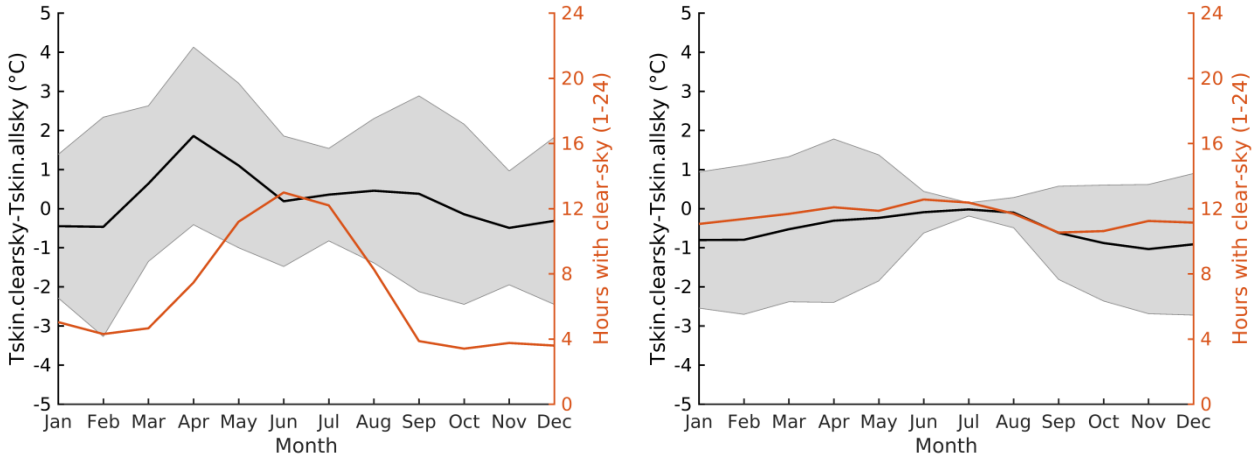

Figure 13: Differences between 24 h averaged clear-sky and all-sky skin temperatures for ACC stations (a) and LAB stations (b) for each month. The red lines show the 24 h average number of hours with CCF>0.7 per day for each month.

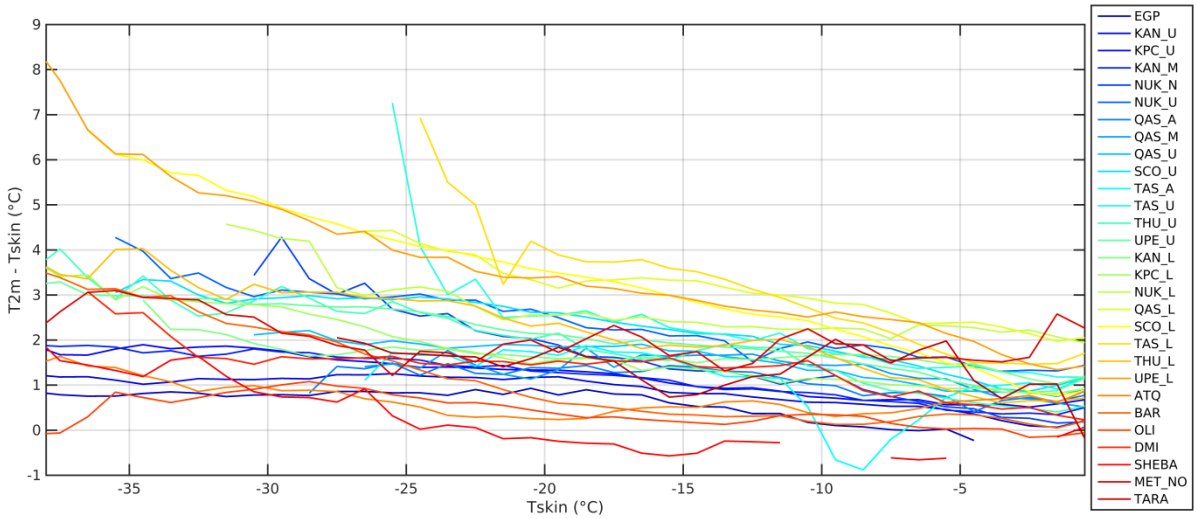

Figure 14: Mean 2 m air temperature and skin temperature differences for all sites as a function of binned skin temperature. The Tskin bin size is 1°C, the T2m-Tskin bin size is 1°C, and only bins with more than 50 members are considered.